Multilevel Focus+Context Visualization using Balanced Multiresolution

Mahmudul Hasan*, Faramarz F. Samavati†, Christian Jacob‡
*†‡*Department of Computer Science*
‡*Department of Biochemistry & Molecular Biology*
University of Calgary, Calgary, Alberta, Canada
{*mhasan, samavati, cjacob*}*@ucalgary.ca*

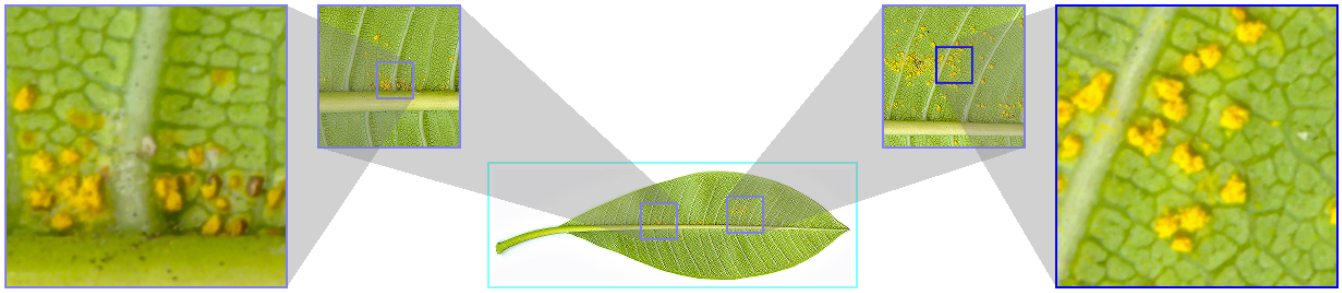

Figure 1: Multilevel focus+context visualization of a Plumeria rubra leaf with frangipani rust. Source image: 10496×3328 (S. Fraser-Smith, Wikipedia).

***Abstract*—In this paper, we present the construction of a multilevel focus+context visualization framework for the navigation and exploration of large-scale 2D and 3D images. The presented framework utilizes a *balanced multiresolution* (BMR) technique supported by a *balanced wavelet transform* (BWT). This devised framework extends the mode of focus+context visualization, where spatially separate magnification of *regions of interest* (ROIs) is performed, as opposed to in-place magnification. Each resulting visualization scenario resembles a tree structure, where the root constitutes the main context, each non-root internal node plays the dual roles of both focus and context, and each leaf solely represents a focus. We use the local multiresolution filters of quadratic B-spline to construct the BWT. Our developed prototype supports interactive manipulation of the visualization hierarchy, such as addition and deletion of ROIs and desired changes in their resolutions at any level of the hierarchy on the fly. Changes in the spatial locations of query windows that define the ROIs trigger on-demand reconstruction queries. We describe in detail how to efficiently process such reconstruction queries within the hierarchy of *details* (wavelet coefficients) contained in the BWT in order to ensure real-time feedback. As the BWT need only be constructed once in a preprocessing phase on the server-side and robust on-demand reconstruction queries require minimal data communication overhead, our presented framework is a suitable candidate for efficient web-based visualization and exploration of complex large-scale imagery.**

***Keywords*-focus+context visualization; contextual close-up; multilevel visualization; multilevel hierarchy; multiscale visualization; balanced multiresolution; balanced decomposition; perfect reconstruction; balanced wavelet transform**

I. Introduction

The continuous growth of 2D/3D image size in various application domains and the prolific use of handheld devices mandate the ability to visualize and explore large-scale images within the physical and ergonomic limitations of the screen space available on such devices. To address this issue, in this paper, we present a multilevel focus+context visualization framework for large-scale 2D and 3D images. The advantages of such a visualization framework are manifold. It allows for more manageable utilization of screen space by the creation of a multilevel visualization hierarchy. In such a multilevel hierarchy, enlarged *regions of interest* (ROIs) can also serve as contexts to further increase the depth of the hierarchy, if required. Therefore, such a hierarchy permits the visualization of contexts with higher *degrees of interest* [1] in higher resolutions, while maintaining interactive frame rates. The ability to have multiple ROIs at different desired resolutions also enables users to draw comparisons between ROIs when applicable.

Query window-based focus+context visualization is useful for the visualization and exploration of large-scale 2D and 3D images. It allows simultaneous visualization of both the local and global views of the data, possibly at varying scales. Facilitating such visualization involves rendering a low-resolution approximation of data providing the context and a high-resolution approximation of an enclosed ROI selected by a query window, defining the focus. The work presented in this paper extends this mode of focus+context visualization to construct a multilevel focus+context visualization framework. See Figure 1 for an example visualization scenario supported by our presented framework.

Such a visualization framework can be supported by a multiresolution data visualization approach, allowing different levels of detail of the data to be properly retrieved, scaled, and rendered at different resolutions on demand. Wavelet transform representations can be exploited to produce coarse approximations of data while retaining the ability to recover the original data when more detail is desired. This can enhance the overall visualization throughput by

removing excessive details unless required. Additionally, wavelet transformation ensures a linear runtime for decomposition and reconstruction with no additional storage requirements.

In order to support the presented visualization framework by an underlying wavelet transform, on-demand reconstruction of high-resolution approximations of the ROIs from low-resolution approximations of data and their corresponding details (wavelet coefficients) is required. Here we exploit a *balanced wavelet transform* (BWT) by means of a *balanced multiresolution* (BMR) technique that provides efficient and straightforward access to details on demand [2]. Notably, it only makes use of regular multiresolution filters, completely eliminating the need for any extraordinary boundary filters.

Such a framework can be used to efficiently support web-based visualization and exploration of complex large-scale imagery on handheld devices with limited screen spaces. This is made possible by the BWT, which need only be constructed once (for each image) on the server-side in a preprocessing phase and allows robust on-demand reconstruction queries to be performed with minimal communication overhead using the *L-updating* technique described later in this paper. Furthermore, *scalability and multilevel hierarchy* was highlighted as one of the top ten challenges regarding *interaction and user interfaces* in extreme-scale visual analytics by Wong *et al.* [3]. We envision that our presented framework for large-scale image visualization and exploration will provide insights toward developing similar visualization frameworks suitable for extreme-scale visual analytics.

The operations we specify for pixels in this paper are readily applicable to voxels. So from this point forward, we generally refer to pixels and voxels as *samples*.

This paper is organized as follows. In section II, we present the notations used throughout the paper for multiresolution operations. Next, a brief survey of related work follows in section III. Section IV presents the construction of our multilevel focus+context visualization framework. In section V, we present the experimental results produced by our developed prototype and section VI concludes the paper with directions for future work.

II. Notation

The paper adopts and extends the notations for denoting multiresolution operations used by Samavati *et al.* in [4].

Decomposition. Given a column vector of fine samples C^k, a column vector of coarse samples C^{k-1} is obtained by downsampling C^k using the matrix equation

$$C^{k-1} = \mathbf{A}^k C^k, \tag{1}$$

and the *details* lost due to downsampling, denoted by D^{k-1} are captured using the matrix equation

$$D^{k-1} = \mathbf{B}^k C^k. \tag{2}$$

$\mathbf{A}^k$ and $\mathbf{B}^k$ used in equations (1) and (2) are decomposition (analysis) filter matrices. This process of deriving C^{k-1} and D^{k-1} from C^k is referred to as *decomposition*. Note that for image decomposition, the sequences of samples along each dimension can be treated independently, allowing any such sequence to form C^k for decomposition.

Reconstruction. The *reconstruction* process involves recovering the column vector of fine samples C^k from the column vectors of coarse sample C^{k-1} and corresponding details D^{k-1}. Reconstruction (synthesis) filter matrices $\mathbf{P}^k$ and $\mathbf{Q}^k$ respectively refine C^{k-1} and D^{k-1} to recover C^k as follows:

$$C^k = \mathbf{P}^k C^{k-1} + \mathbf{Q}^k D^{k-1}. \tag{3}$$

Equation (3) reverses the application of decomposition filter matrices $\mathbf{A}^k$ and $\mathbf{B}^k$ on the original column vector of fine samples C^k. So decomposition and reconstruction are inverse processes that satisfy

$$\begin{bmatrix} \mathbf{A}^k \\ \mathbf{B}^k \end{bmatrix} \begin{bmatrix} \mathbf{P}^k & \mathbf{Q}^k \end{bmatrix} = \begin{bmatrix} \mathbf{I} & \mathbf{0} \\ \mathbf{0} & \mathbf{I} \end{bmatrix}.$$

Wavelet transform. Recursive decompositions of a column vector of fine samples C^k into column vectors of coarse samples $C^l, C^{l+1}, \ldots, C^{k-1}$ and corresponding details $D^l, D^{l+1}, \ldots, D^{k-1}$ construct the *wavelet transform* of C^k, denoted by $C^l, D^l, D^{l+1}, \ldots, D^{k-1}$, where $l < k$. From this wavelet transform, we can fully or partially reconstruct each of $C^{l+1}, \ldots, C^{k-1}, C^k$.

Simplified notations. For the rest of the paper, we simplify the notations by omitting the superscript k for the kth level of resolution with the following assumptions: $F = C^k$, $C = C^{k-1}$, $D = D^{k-1}$, $\mathbf{A} = \mathbf{A}^k$, and $\mathbf{B} = \mathbf{B}^k$, $\mathbf{P} = \mathbf{P}^k$, and $\mathbf{Q} = \mathbf{Q}^k$. Also, the decomposition and reconstruction filter matrices are assumed to have appropriate sizes to satisfy the equations

$$C = \mathbf{A}F, \tag{4}$$

$$D = \mathbf{B}F, \tag{5}$$

$$F = \mathbf{P}C + \mathbf{Q}D. \tag{6}$$

The filter matrices $\mathbf{A}$, $\mathbf{B}$, $\mathbf{P}$ and $\mathbf{Q}$ we consider are of banded, repetitive, and slanted structure. So, let the nonzero entries in a representative row of $\mathbf{A}$ and $\mathbf{B}$ be represented by decomposition filter vectors $\mathbf{a}$ and $\mathbf{b}$, respectively. In a similar manner, let the nonzero entries in a representative column of $\mathbf{P}$ and $\mathbf{Q}$ be denoted by reconstruction filter vectors $\mathbf{p}$ and $\mathbf{q}$, respectively.

III. Related Work

The following two subsections present a brief review of existing related work on multiresolution and focus+context visualization.

A. Multiresolution

Due to the regular structure of images, multiresolution methods applicable to curves and regular meshes (tensor-product surfaces and volumes) are also applicable to images. A mathematically clean and efficient approach to multiresolution based on reverse subdivision was made possible due to the work of Samavati and Bartels [5], [6], [7]. For decomposition, their approach involves obtaining each coarse vertex through an efficient local least squares optimization, which reduces undesired undulations. Furthermore, compared to the conventional wavelets for curves and regular surfaces, the wavelets resulting from this approach provide a more compact support. The multiresolution filters we used to produce the experimental results in section V were derived using this approach.

Conventional multiresolution schemes for the local filters of second or higher order scaling functions and their wavelets lead to unequal numbers of coarse and detail samples after decomposition. This inequality makes locating the details required for the on-demand reconstruction of an enlarged ROI in a multilevel visualization hierarchy cumbersome. Furthermore, such multiresolution schemes may need to use extraordinary boundary filters in order to handle image and detail boundaries. This makes the reconstruction of ROI sub-regions near image boundaries computationally untidy. In order to address these issues, Hasan *et al.* recently introduced a technique for devising BMR schemes for a class of multiresolution filter vectors that are *symmetric/antisymmetric* about their centers [2].

The use of a wavelet tree [8], octree-based hierarchies [9], [10], [11], and resampling based on space deformation [12] are noteworthy existing approaches supporting context-aware multiresolution visualization of 3D images. The wavelet-based time-space partitioning (WTSP) tree was utilized for 4D images in [8]. In order to support context-aware multiresolution visualization of a 2D or 3D image, we construct its BWT as suggested in [2], which compactly stores a coarse approximation of the image in addition to a hierarchy of details (see Figure 2, for example).

B. Focus+Context Visualization

Hauser generalized focus+context visualization across the fields of information and scientific visualizations based on the various methods (such as graphics resource allocation) used to discriminate between data subsets corresponding to focus and context [13]. Using a metaphor of lenses is a prominent way of supporting focus+context visualization [14], [15], [12]. This technique is influenced by traditional handcrafted medical, technical, and scientific illustrations [16]. According to the categorization by Cohen and Brodlie [17], our implemented multiresolution approach to this metaphor of lenses is discontinuous and undistorted like that in [14], as opposed to continuous and distorted techniques in [15], [12].

Multifocal and/or multicontext visualization techniques have been used in the literature for various types of data. Cossalter *et al.* used a multifocal multilevel technique for network visualizations [18]. Tu and Shen presented a multifocal technique applicable to treemap visualizations for hierarchical data [19]. Mendez *et al.* used a multifocal [20] and Kalkofen *et al.* a multicontext [21] approach to focus+context visualization in augmented reality applications. Ropinski *et al.* made use of a multifocal approach, utilizing multiple interactive closeups for the visualization of multiple modalities of medical data [22]. In contrast to this body of work, we take a multiresolution approach to interactive multilevel focus+context visualization, supported by an underlying BWT.

IV. Methodology

We support our multilevel focus+context visualization framework using an underlying BWT constructed by a BMR scheme for two reasons. Firstly, a BWT provides straightforward access to details corresponding to a ROI in a multilevel hierarchy. Secondly, a BMR scheme does not require any extraordinary boundary filters, the use of which leads to computationally untidy reconstruction of ROI sub-regions near image boundaries. Additionally, we present an efficient technique for processing reconstruction queries to ensure real-time feedback and a sample normalization and quantization method we adopted for rendering purposes.

A. Balanced Multiresolution (BMR)

We utilize a BMR scheme devised according to the construction procedure presented in [2]. Using a given set of regular multiresolution filter vectors $\mathbf{a}$, $\mathbf{b}$, $\mathbf{p}$, and $\mathbf{q}$ that are symmetric/asymmetric in structure, a BMR scheme allows for a balanced decomposition and a subsequent perfect reconstruction of a dataset. Here, balanced decomposition is defined such that $size(C) = size(D) = size(F)/2$, where $size(\ldots)$ returns the number of elements in the argument vector.

A BMR scheme avoids the use of extraordinary boundary filters using an extended version of the column vector of fine samples F for decomposition and, similarly, extended versions of the column vectors of coarse samples C and detail samples D for reconstruction. Let F' denote the extended version of F, obtained through symmetric extensions at the boundaries. Also, let C' and D' denote the extended versions of C and D, respectively, obtained through symmetric/antisymmetric extensions at their boundaries. Then the decomposition and reconstruction processes of a BMR scheme are governed by the equations

$$C = \mathbf{A}F', \tag{7}$$

$$D = \mathbf{B}F', \tag{8}$$

$$F = \mathbf{P}C' + \mathbf{Q}D', \tag{9}$$

analogous to equations (4), (5), and (6), respectively.

Multiresolution filters. The BMR scheme we use is devised using the *short* local filters of quadratic (third order) B-spline:

$$\begin{cases} \mathbf{a} = \begin{bmatrix} a_{-2} & a_{-1} & a_1 & a_2 \end{bmatrix} = \begin{bmatrix} -\frac{1}{4} & \frac{3}{4} & \frac{3}{4} & -\frac{1}{4} \end{bmatrix}, \\ \mathbf{b} = \begin{bmatrix} b_{-2} & b_{-1} & b_1 & b_2 \end{bmatrix} = \begin{bmatrix} \frac{1}{4} & -\frac{3}{4} & \frac{3}{4} & -\frac{1}{4} \end{bmatrix}, \\ \mathbf{p} = \begin{bmatrix} p_{-2} & p_{-1} & p_1 & p_2 \end{bmatrix} = \begin{bmatrix} \frac{1}{4} & \frac{3}{4} & \frac{3}{4} & \frac{1}{4} \end{bmatrix}, \\ \mathbf{q} = \begin{bmatrix} q_{-2} & q_{-1} & q_1 & q_2 \end{bmatrix} = \begin{bmatrix} -\frac{1}{4} & -\frac{3}{4} & \frac{3}{4} & \frac{1}{4} \end{bmatrix}. \end{cases} \tag{10}$$

The filter vectors in (10) were constructed by reversing Chaikin subdivision [23] in [4]. Note that they are symmetric/antisymmetric about their centers, as required for setting up a BMR scheme.

Balanced decomposition. Following the general construction for a balanced decomposition in [2], for a column vector of fine samples $F = [f_1 \; f_2 \; \ldots \; f_{2n}]^T$ where $n \in \mathbb{Z}^+$, we obtain $F' = [f_1 \; f_1 \; \ldots \; f_{2n} \; f_{2n}]^T$ through half-sample symmetric extensions at the two boundaries of F. Then the column vectors of coarse samples $C = [c_1 \; c_2 \; \ldots \; c_n]^T$ and detail samples $D = [d_1 \; d_2 \; \ldots \; d_n]^T$ are obtained as follows:

$$\begin{cases} c_1 &= a_{-2}f_1 + a_{-1}f_1 + a_1 f_2 + a_2 f_3, \\ d_1 &= b_{-2}f_1 + b_{-1}f_1 + b_1 f_2 + b_2 f_3, \\ \vdots & \\ c_i &= a_{-2}f_{2i-2} + a_{-1}f_{2i-1} + a_1 f_{2i} + a_2 f_{2i+1}, \\ d_i &= b_{-2}f_{2i-2} + b_{-1}f_{2i-1} + b_1 f_{2i} + b_2 f_{2i+1}, \\ \vdots & \\ c_n &= a_{-2}f_{2n-2} + a_{-1}f_{2n-1} + a_1 f_{2n} + a_2 f_{2n}, \\ d_n &= b_{-2}f_{2n-2} + b_{-1}f_{2n-1} + b_1 f_{2n} + b_2 f_{2n}, \end{cases} \tag{11}$$

for $i = 2 \ldots (n-1)$. Note that (11) shows a linear evaluation of C and D using matrix equations (7) and (8), respectively.

Balanced decomposition along one or more dimensions of an image for a desired number of levels creates the corresponding BWT. For the purpose of demonstration, Figure 2 shows the BWT resulting after two levels of heightwise and widthwise balanced decompositions of a 1024×512 Blue Marble image. Note that in practice, images that require multilevel focus+context visualization are larger in size.

Perfect reconstruction. According to the general construction for a perfect reconstruction provided in [2], we obtain $C' = [c_1 \; c_1 \; \ldots \; c_n \; c_n]^T$ using half-sample symmetric extensions at the two boundaries of C and $D' = [-d_1 \; d_1 \; \ldots \; d_n \; -d_n]^T$ using half-sample antisymmetric extensions at the two boundaries of D. Then the column vector of fine samples F is reconstructed from C' and D' as follows:

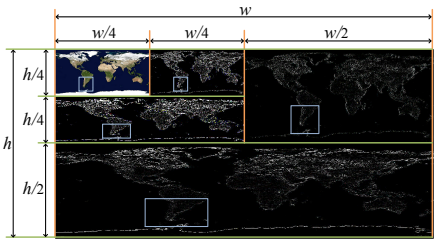

Figure 2: BWT of a $w \times h$ Blue Marble image after two levels of balanced decomposition, with rectangles enclosing all levels of details corresponding to a ROI in the coarse approximation of the image (in the top-left corner). Source image: 1024×512 (Visible Earth, NASA).

$$\begin{cases} f_1 &= p_2 c_1 + p_{-1}c_1 + q_2(-d_1) + q_{-1}d_1, \\ \vdots & \\ f_{2i} &= p_1 c_i + p_{-2}c_{i+1} + q_1 d_i + q_{-2}d_{i+1}, \\ f_{2i+1} &= p_2 c_i + p_{-1}c_{i+1} + q_2 d_i + q_{-1}d_{i+1}, \\ \vdots & \\ f_{2n} &= p_1 c_n + p_{-2}c_n + q_1 d_n + q_{-2}(-d_n), \end{cases} \tag{12}$$

for $i = 1 \ldots (n-1)$. Observe that (12) shows a linear evaluation of F using the matrix equation (9).

B. Reconstruction Queries

Locating details. For processing reconstruction queries in our multilevel focus+context visualization framework, we need to perform on-demand reconstruction of context subregions that define the ROIs from an underlying BWT. To do this, we need to locate the details corresponding to each ROI. Figure 2 shows a ROI in the coarse approximation of an image and corresponding details contained within the BWT. Regardless of what level of the visualization hierarchy a ROI is from, the balanced structure of the BWT makes locating the corresponding details straightforward. For instance, observe the reconstruction of interior samples in (12) — if the first coarse sample in the reconstruction of a fine sample is c_i, then d_i is the first detail sample to use in the reconstruction of that fine sample. Furthermore, that fine sample is either f_{2i} or f_{2i+1} depending on which reconstruction filters are used.

Avoiding redundant reconstructions. Depending on the depth of the multilevel visualization hierarchy where a moving query window (defining changing ROIs) is located, the triggered reconstruction queries can become computationally expensive. This negatively affects the ability to provide real-time feedback. To address this issue, here we describe an *L-updating* technique we employed to avoid redundant reconstruction operations. It works in a manner similar to clipmap-update for terrain rendering performed by Losasso and Hoppe, where they utilized L-like clip regions [24].

We explain the concept of L-updating for 2D images, which is extendable to work with 3D images in a straight-

forward manner. The ROI in a coarse approximation of a 2D image is identified by a movable rectangular query window. Figure 3(a) shows four configurations of how such a query window can move. In each configuration, the rectangles with black and blue edges represent the old and new locations of the query window before and after a move, respectively. The rectangular area shaded in orange represents the intersection between the old and new ROIs for each configuration. The signed dx and dy values represent the direction and magnitude of the move made by the query window.

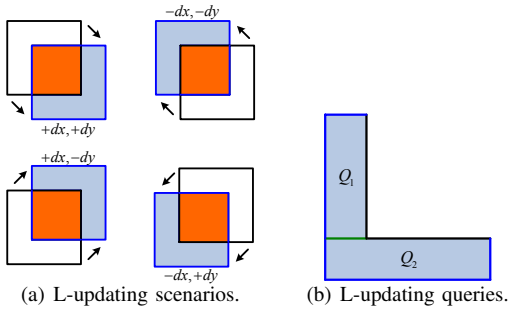

(a) L-updating scenarios. (b) L-updating queries.

Figure 3: The L-updating technique.

In most scenarios, the old and new ROIs intersect. Provided that the high-resolution approximation of the old ROI has already been reconstructed, the high-resolution approximation for the intersection region (shown in orange for the each scenario in Figure 3(a)) can be reused directly from the old enlarged ROI while obtaining the new enlarged ROI. Therefore, for each scenario, we only need to reconstruct the high-resolution approximation for the L-like polygonal area of the new ROI shaded in light-blue.

In order to reconstruct the high-resolution approximation for the L-like polygonal area of the new ROI, we break it down into two rectangular reconstruction queries, Q_1 and Q_2, as shown in Figure 3(b). Note that if either dx or dy is zero, then there will be only one reconstruction query instead. From the standpoint of implementation, the same memory area can be used to update the high-resolution approximation of the old ROI into the high-resolution approximation of the new ROI. This process involves shifting the reusable high-resolution approximation of the old ROI to the opposite corner (observe in Figure 3(a)) and copying the results of Q_1 and Q_2 to the appropriate locations.

The L-updating technique significantly reduces the computational overhead by eliminating redundant reconstruction operations. While exploiting a three-dimensional query probe for interactive visualization and exploration of 3D images, utilizing the L-updating technique can result in a substantial gain in performance. It can also greatly minimize the data communication overheads in applications of our presented framework to web-based visualization and exploration of large-scale imagery.

Data structure. We need to keep track of the tree-like structure of visualization scenarios supported by our presented framework. For this purpose, we make use of a *left-child right-sibling* binary tree, which allows us to efficiently store pertinent information in a one-dimensional array regardless of the number of query windows a context window might contain. For instance, Figure 4(a) shows the binary tree corresponding to the displayed visualization scenario, where the main context and the enlarged ROIs are marked with letters A through F. Each node in the tree other than the root is used to store the high-resolution approximation of the corresponding ROI for rendering and further reconstruction purposes, in addition to some relevant information such as its location in the main context, screen coordinates, etc.

C. Sample Normalization and Quantization

When a decomposition filter value is applied to a sample, it is applied independently to each of its components (such as red, green, and blue). The resulting sample will usually have each of its components as floating point values, which must be stored to ensure a perfect (lossless) reconstruction. These floating point values may also fall outside the interval of $[0, iMax]$, where $iMax$ is the maximum integer intensity value. However, for rendering purposes, these floating point values must be mapped to the integer range of 0 to $iMax$. A simple strategy for normalization is to replace the floating point values less than the minimum intensity of 0 with 0 and greater than the maximum intensity $iMax$ with $iMax$. Rounding up or down according to a preset criterion can quantize the floating point values between 0 and $iMax$. For the purpose of rendering, we obtain an integer intensity value i from a floating point value f as follows:

$$i = \begin{cases} 0 & \text{if } f \leq 0, \\ \lfloor f \rfloor & \text{if } 0 < f < iMax \wedge (f - \lfloor f \rfloor) \leq 0.5, \\ \lceil f \rceil & \text{if } 0 < f < iMax \wedge (f - \lfloor f \rfloor) > 0.5, \\ iMax & \text{if } f \geq iMax. \end{cases} \quad (13)$$

The experimental results provided in section V are rendered using the conditions in (13). Other commonly used approaches involve uniformly mapping either the precalculated possible interval or the actual interval of the resulting floating point values to the integer range of 0 to $iMax$. These approaches have varying impacts on the contrast of the resulting images.

One can avoid this normalization and quantization step by using multiresolution filters that map integer samples to integer samples. However, devising BMR schemes based on such multiresolution filters still remains unexplored.

V. Results

We have developed a visualization tool prototype to validate our presented multilevel focus+context visualization framework for images. In Figures 4 and 5, the associated levels of decomposition and reconstruction are shown at the

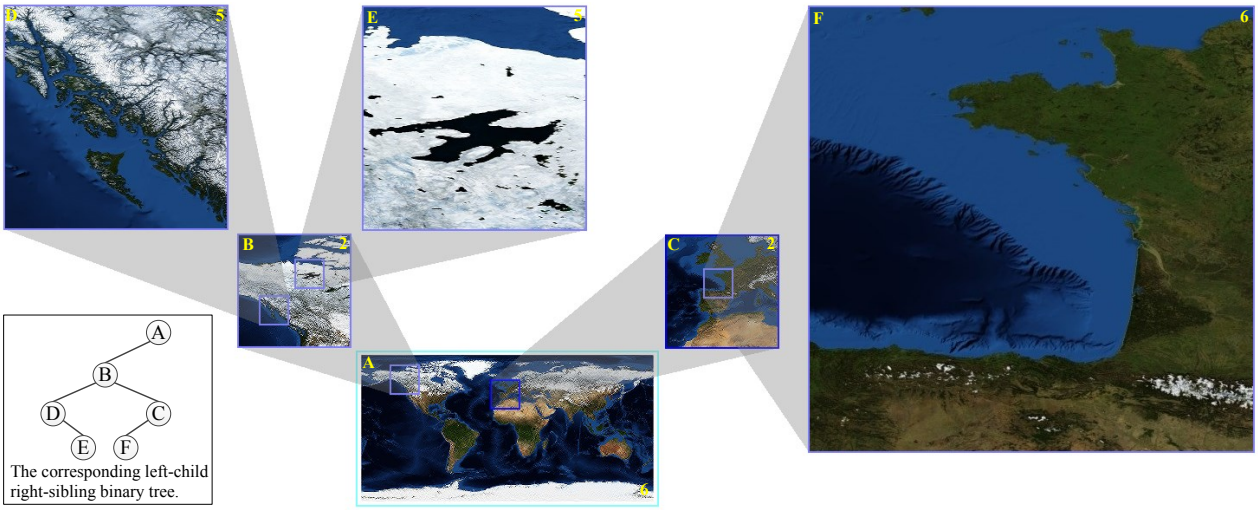

(a) Blue Marble topography and bathymetry. Source image: 21632×10816 (Visible Earth, NASA).

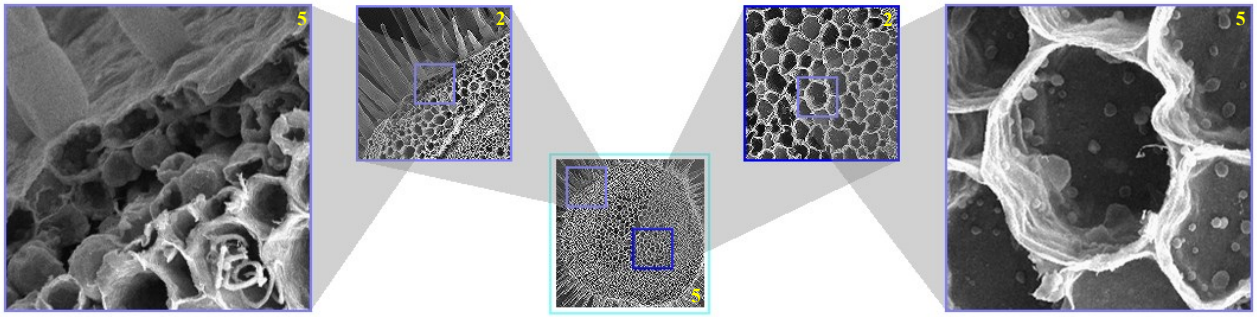

(b) Nicotiana alata stem cross section. Source image: 4000×4000 (Dartmouth Electron Microscope Facility).

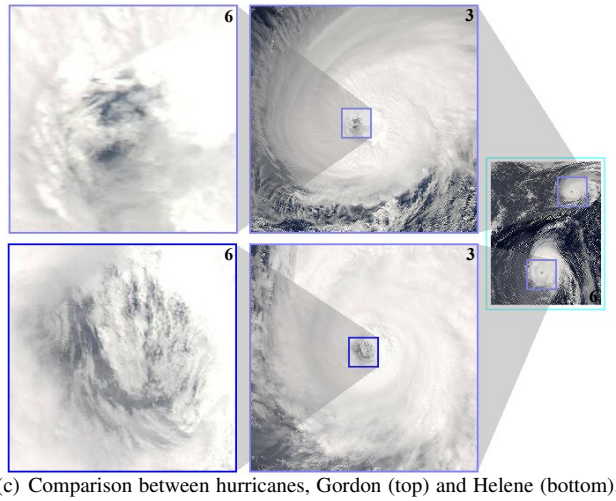

(c) Comparison between hurricanes, Gordon (top) and Helene (bottom). Source image: 8000×10432 (NASA/GSFC, MODIS Rapid Response).

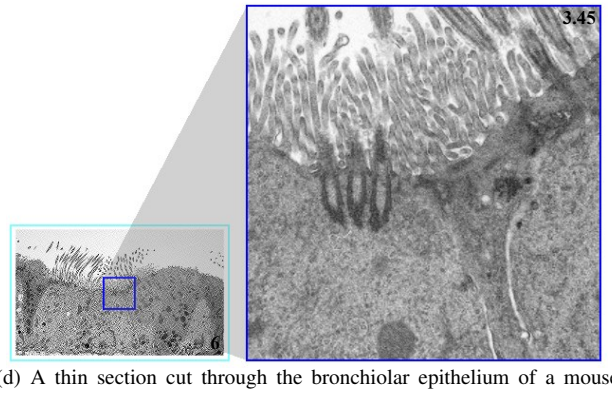

(d) A thin section cut through the bronchiolar epithelium of a mouse lung. Source image: 14080×8512 (Dartmouth Electron Microscope Facility).

Figure 4: Various focus+context visualization scenarios for 2D images.

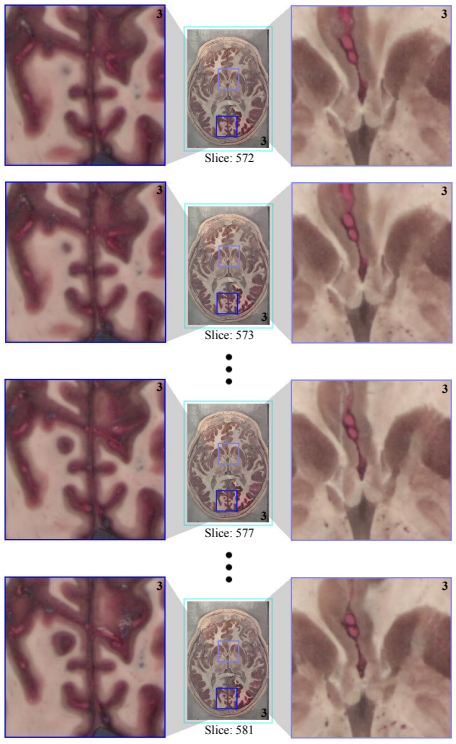

Figure 5: A fly-through focus+context visualization scenario for a 3D image. Source image: $1056 \times 1528 \times 150$ (Part of the male's head from the Visible Human Project, U.S. National Library of Medicine).

bottom-right corner of each main context and at the top-right corner of each enlarged ROI, respectively.

Figure 4 shows several focus+context visualization and exploration scenarios for 2D images facilitated by our developed tool. Figures 4(a) and 4(b) present multilevel focus+context visualization of Earth's topography and bathymetry on a Blue Marble image and the cross section of the stem of a Nicotiana alata plant, respectively. Figure 4(c) draws a comparison between hurricanes, Gordon and Helene that appeared in September 2006. Our developed prototype also allows fractional changes in the resolution of an enlarged ROI through trilinear interpolation between two consecutive integer resolutions of the ROI; Figure 4(d) shows such a ROI at floating point resolution 3.45, magnifying a part of a thin layer cut from the bronchiolar epithelium of a mouse lung.

Our prototype allows focus+context visualization and exploration of a 3D image by means of interactive depthwise transitions of query windows defining the ROIs. Such transitions are controlled by the user either through the use of the attached mouse scroll wheel or the up and down arrow keys on the attached keyboard. Currently, our prototype only performs widthwise and heightwise decompositions of 3D images, keeping the number of 2D slices along the depth constant for depthwise volume exploration. Figure 5 presents such a visualization scenario created in our prototype. For the sake of demonstration, it only shows the fly-through transition of two query windows through ten of the 150 sequential slices loaded into our prototype for this visualization task. The dimensions of the original dataset are $1056 \times 1528 \times 1477$. In a similar manner, our developed prototype can also process large-scale time-lapse imagery, constraining the query windows to move back and forth along the time dimension.

The runtimes for the performed decomposition and reconstruction operations are linear on the number of processed samples. For our implementation, the memory usage is linear on the total number of samples in the source image and the enlarged ROIs.

VI. Conclusion and Future Work

In this paper, we presented a multilevel focus+context visualization framework for effective and manageable navigation and exploration of large-scale 2D and 3D images. Our presented framework extends the discontinuous and undistorted mode of focus+context visualization based on an underlying BWT, utilized by means of a BMR scheme. The BMR scheme we used is devised based on the local multiresolution filters of quadratic B-spline. Unlike preexisting multiresolution approaches to focus+context visualization, our use of a BMR scheme facilitates straightforward access to details required for on-demand reconstruction of enlarged ROIs and allows us to avoid the use of extraordinary boundary filters.

We also described an *L-updating* technique that ensures real-time feedback by avoiding redundant reconstruction operations while processing reconstruction queries triggered by a moving query window defining changing ROIs. Our developed prototype allows real-time exploration of large-scale images through interactive manipulation of the visualization hierarchy.

With the growth of data size, the increasing depth of a multilevel visualization hierarchy supported by a multilevel focus+context framework may cause user disorientation. To address this issue, an important direction for future work involves augmenting enlarged ROIs with supplementary textual and visual information in order to reduce user disorientation. This direction for future work is also aligned with the *scalability and multilevel hierarchy* challenge identified in [3], that highlights the navigation of deep multilevel hierarchies and identifying optimal resolutions (for ROIs, in our context) as major challenges.

Acknowledgment

This research received generous support from the *Natural Sciences and Engineering Research Council* (NSERC) of Canada, *Alberta Innovates – Technology Futures* (AITF), *Alberta Enterprise and Advanced Education*, and *Networks of Centres of Excellence* (NCE) of Canada in *Graphics,*

Animation and New Media (GRAND). We would like to thank Mario Costa Sousa for his insightful discussions and Troy Alderson for his helpful editorial comments.

REFERENCES

[1] S. K. Card and D. Nation, "Degree-of-interest trees: A component of an attention-reactive user interface," in *Proceedings of the Working Conference on Advanced Visual Interfaces*, ser. AVI '02. New York, NY, USA: ACM, 2002, pp. 231–245.

[2] M. Hasan, F. F. Samavati, and M. C. Sousa, "Balanced multiresolution for symmetric/antisymmetric filters," Department of Computer Science, University of Calgary, Calgary, Alberta, Canada, Tech. Rep. 2014-1059-10, May 2014. [Online]. Available: http://hdl.handle.net/1880/49997

[3] P. C. Wong, H.-W. Shen, C. Johnson, C. Chen, and R. B. Ross, "The top 10 challenges in extreme-scale visual analytics," *IEEE Computer Graphics and Applications*, vol. 32, no. 4, pp. 63–67, Jul 2012.

[4] F. F. Samavati, R. H. Bartels, and L. Olsen, "Local B-spline multiresolution with examples in iris synthesis and volumetric rendering," in *Image Pattern Recognition: Synthesis and Analysis in Biometrics*, ser. Machine Perception and Artificial Intelligence, S. N. Yanushkevich, M. L. Gavrilova, P. S. P. Wan, and S. N. Srihari, Eds. World Scientific Publishing, 2007, vol. 67, no. 3, pp. 65–102.

[5] F. F. Samavati and R. H. Bartels, "Multiresolution curve and surface representation: reversing subdivision rules by least-squares data fitting," *Computer Graphics Forum*, vol. 18, no. 2, pp. 97–119, 1999.

[6] R. H. Bartels, G. H. Golub, and F. F. Samavati, "Some observations on local least squares," *BIT Numerical Mathematics*, vol. 46, no. 3, pp. 455–477, Sep 2006.

[7] R. Bartels and F. Samavati, "Multiresolutions numerically from subdivisions," *Computers & Graphics*, vol. 35, no. 2, pp. 185–197, 2011.

[8] C. Wang and H.-W. Shen, "Hierarchical navigation interface: leveraging multiple coordinated views for level-of-detail multiresolution volume rendering of large scientific data sets," in *Proceedings of the Ninth International Conference on Information Visualisation*, Jul 2005, pp. 259–267.

[9] E. LaMar, B. Hamann, and K. I. Joy, "Multiresolution techniques for interactive texture-based volume visualization," in *Proceedings of the 1999 Conference on Visualization*, ser. VIS '99. Los Alamitos, CA, USA: IEEE Computer Society Press, 1999, pp. 355–361.

[10] J. Plate, M. Tirtasana, R. Carmona, and B. Fröhlich, "Octreemizer: a hierarchical approach for interactive roaming through very large volumes," in *Proceedings of the Symposium on Data Visualisation 2002*, ser. VISSYM '02. Aire-la-Ville, Switzerland: Eurographics Association, 2002, pp. 53–60.

[11] S. Suter, J. I. Guitian, F. Marton, M. Agus, A. Elsener, C. Zollikofer, M. Gopi, E. Gobbetti, and R. Pajarola, "Interactive multiscale tensor reconstruction for multiresolution volume visualization," *IEEE Transactions on Visualization and Computer Graphics*, vol. 17, no. 12, pp. 2135–2143, Dec 2011.

[12] Y.-S. Wang, C. Wang, T.-Y. Lee, and K.-L. Ma, "Feature-preserving volume data reduction and focus+context visualization," *IEEE Transactions on Visualization and Computer Graphics*, vol. 17, no. 2, pp. 171–181, Feb 2011.

[13] H. Hauser, "Generalizing focus+context visualization," in *Scientific Visualization: The Visual Extraction of Knowledge from Data*, ser. Mathematics and Visualization, G.-P. Bonneau, T. Ertl, and G. Nielson, Eds. Springer Berlin Heidelberg, 2006, pp. 305–327.

[14] T. Taerum, M. C. Sousa, F. F. Samavati, S. Chan, and J. R. Mitchell, "Real-time super resolution contextual close-up of clinical volumetric data," in *Proceedings of the Joint Eurographics – IEEE VGTC Symposium on Visualization*, ser. EuroVis '06. Eurographics Association, May 8-10 2006, pp. 347–354.

[15] W.-H. Hsu, K.-L. Ma, and C. Correa, "A rendering framework for multiscale views of 3D models," in *Proceedings of the 2011 SIGGRAPH Asia Conference*, ser. SA '11. New York, NY, USA: ACM, 2011, pp. 131:1–131:10.

[16] E. R. S. Hodges, *The Guild handbook of scientific illustration*. Hoboken, NJ, USA: John Wiley and Sons, 2003.

[17] M. Cohen and K. Brodlie, "Focus and context for volume visualization," in *Proceeding of the 2004 Theory and Practice of Computer Graphics Conference*, Jun 2004, pp. 32–39.

[18] M. Cossalter, O. J. Mengshoel, and T. Selker, "Multi-focus and multi-level techniques for visualization and analysis of networks with thematic data," in *Proceeding of the SPIE Conference on Visualization and Data Analysis*, vol. 8654, Feb 2013, pp. 1–15, 865403.

[19] Y. Tu and H.-W. Shen, "Balloon focus: A seamless multi-focus+context method for treemaps," *IEEE Transactions on Visualization and Computer Graphics*, vol. 14, no. 6, pp. 1157–1164, 2008.

[20] E. Mendez, D. Kalkofen, and D. Schmalstieg, "Interactive context-driven visualization tools for augmented reality," in *IEEE/ACM International Symposium on Mixed and Augmented Reality*, ser. ISMAR '06, Oct 2006, pp. 209–218.

[21] D. Kalkofen, E. Mendez, and D. Schmalstieg, "Interactive focus and context visualization for augmented reality," in *IEEE/ACM International Symposium on Mixed and Augmented Reality*, ser. ISMAR '07, Nov 2007, pp. 191–201.

[22] T. Ropinski, I. Viola, M. Biermann, H. Hauser, and K. Hinrichs, "Multimodal visualization with interactive closeups," in *Proceeding of the 2009 Theory and Practice of Computer Graphics Conference*, 2009, pp. 17–24.

[23] G. M. Chaikin, "An algorithm for high-speed curve generation," *Computer Graphics and Image Processing*, vol. 3, no. 4, pp. 346–349, 1974.

[24] F. Losasso and H. Hoppe, "Geometry clipmaps: Terrain rendering using nested regular grids," in *ACM SIGGRAPH 2004 Papers*, ser. SIGGRAPH '04. New York, NY, USA: ACM, 2004, pp. 769–776.